NUCL SCI TECH (2019) 30:104
https://doi.org/10.1007/s41365-019-0629-8

Effects of systematic octupole coupling resonances

Hong-Jin Zeng[1,2,3,4] · Shyh-Yuan Lee[5] · Shu-Xin Zheng[1,2,3] · Hong-Juan Yao[1,2,3] · Xue-Wu Wang[1,2,3] · Hui Ning[4] · Xiao-Jun Meng[4]

Received: 7 November 2018 / Revised: 22 February 2019 / Accepted: 20 March 2019 / Published online: 3 June 2019

Abstract The Xi'an proton accelerator facility synchrotron lattice has a systematic fourth-order resonance. The systematic octupole component in dipole magnets is found to have no adverse effect on the dynamic aperture in multiparticle tracking. The frequency map shows particles locked onto the $2\nu_x - 2\nu_z = 0$ resonance. However, we will show that the instantaneous betatron tunes can vary widely around the resonance line for particles locked onto the resonance.

Keywords Octupole · Coupling resonance · Dynamic aperture · XiPAF

This work was supported by U.S. National Science Foundation (No. PHY-1504778).

✉ Hong-Jin Zeng
hongjin@pku.edu.cn

Shyh-Yuan Lee
shylee@indiana.edu

Shu-Xin Zheng
zhengsx@tsinghua.edu.cn

[1] Key Laboratory of Particle and Radiation Imaging (Tsinghua University), Ministry of Education, Beijing 100084, China

[2] Laboratory For Advanced Radiation Sources and Application, Tsinghua University, Beijing 100084, China

[3] Department of Engineering Physics, Tsinghua University, Beijing 100084, China

[4] Northwest Institute of Nuclear Technology, Xi'an 710024, China

[5] Department of Physics, Indiana University, Bloomington, IN 47405, USA

1 Introduction

The Xi'an proton accelerator facility (XiPAF) is a 230 MeV high-intensity proton accelerator for medical and radiation-science applications [1]. The design is based on missing dipole FODO cells with six superperiods. The accelerator employs third-order resonant slow extraction for high duty cycle beam operation at the $3\nu_x = 5$ resonance [2, 3]. The initial betatron tunes are $\nu_x = 1.76$ and $\nu_z = 1.81$ at injection [4], tunable up to a range of ± 0.5 for the third-order resonance slow extraction [5]. Figure 1 shows an example of the XiPAF lattice at $\nu_x = 1.757717$ and $\nu_z = 1.812286$.

The XiPAF synchrotron has systematic octupole resonances at $4\nu_x = 6$, $4\nu_z = 6$, $2\nu_x + 2\nu_z = 6$, and $2\nu_x - 2\nu_z = 0$. The betatron tunes are sufficiently far away from the octupole parametric and sum resonances, except for the systematic octupole difference resonance. The effect of the systematic Montague space-charge resonance [6–8] at $2\nu_x - 2\nu_z = 0$ has been carefully studied at injection and during the beam acceleration [9].

In the optimization of the dipole-magnet design, there is a substantial systematic octupole component in all dipole magnets. This study focuses on the effect of the systematic octupole magnetic field on the dynamic aperture and its effects on the performance of the synchrotron.

The frequency-map analysis [10–13] has become a standard tool for particle-beam tracking and dynamic-aperture analysis. When beam particles encounter a nonlinear resonance, the betatron tunes of these particles seem to clump and stay on the resonance line [14], as emphasized by Schmidt in a recent International Committee for Future Accelerators (ICFA) mini-workshop on dynamic apertures of circular accelerators in 2017. This

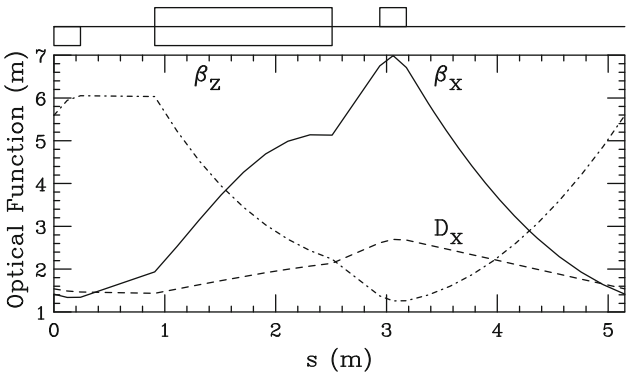

Fig. 1 The optical functions of the XiPAF lattice in one superperiod at $v_x = 1.757717$ and $v_z = 1.812286$

phenomenon is sometimes known as the devil's staircase in nonlinear dynamics. In fact, when particles are trapped in a resonance island, they have a resonance tune. However, each particle in the resonance island may be individually modulated by their motion in the resonance island [15, 16]. Although the tune of particles trapped in resonance islands is the resonance tune, their actual turn-by-turn tune is modulated by the "island tune," exhibited as sidebands around the resonant tune.

This study is intended to examine the effect of the systematic octupole resonance at $2v_x - 2v_z = 0$ on the dynamic aperture of the XiPAF synchrotron and compare the resonant trapping of the coupling resonance line and the actual particle tunes of these particles. We organize this paper as follows. Section 2 studies the effect of the systematic octupole magnetic field on the dynamic aperture. Section 3 details the multiparticle simulations to examine the effect of particles locked onto the coupling resonance. The conclusion is discussed in Sect. 4.

2 Effect of systematic octupoles on dynamic apertures

In the Frenet–Serret coordinate system, the Hamiltonian for particle motion in the presence of octupoles is

$$H = \frac{1}{2}x'^2 + \frac{1}{2}K_x(s)x^2 + \frac{1}{2}z'^2 + \frac{1}{2}K_z(s)z^2 + V_3(s),$$
$$V_3(s) = \frac{K_3(s)}{24}\left(x^4 - 6x^2z^2 + z^4\right), \tag{1}$$

where $K_3(s) = (\partial^3 B_z/\partial x^3)|_{\text{closed-orbit}}/B\rho$, B_z is the vertical component of the magnetic field, and $B\rho$ is the magnetic rigidity of the beam. Because the XiPAF lattice has sixfold symmetry, systematic octupole resonances occur at $4v_x = 6, 4v_z = 6$, $2v_x + 2v_z = 6$ and $2v_x - 2v_z = 0$. The first three resonances are outside the operation range. However, the beam sits near the $2v_x - 2v_z = 0$ resonance. The $K_3(s)$ parameter in XiPAF can be as high as 40m^{-4} at injection. We study the effect of this coupling resonance at the XiPAF.

The dynamic aperture (DA) is normally explored by particle tracking via the magnitude of the "tune diffusion index": $D = \log_{10}\left[\sqrt{(\Delta v_x)^2 + (\Delta v_z)^2}\right]$, where Δv_x and Δv_z are the differences of the betatron tunes evaluated for each particle between the first half and the second half of the tracking turns [10–13]. A stable motion is associated with a small tune diffusion index. The frequency map plots the tune diffusion index versus the initial particle coordinates (x, z) or the betatron tune space (v_x, v_z). The resulting frequency map exhibits resonance lines associated with particle loss or high diffusion index in phase-space locations of the beam. In particular, it appears that particles are locked onto these resonance lines [14]. We use the ELEGANT code [17] to perform DA tracking for the XiPAF. The frequency-map analysis is integrated in the ELEGANT code [18–21]. Figure 2 shows the diffusion index versus the betatron tunes at turn 100 and 1000 at the top, and the diffusion index versus the horizontal and vertical coordinates at the bottom. Additional supporting material in the form of a .gif movie file is included to show the evolution of the frequency map of particles. The betatron tunes of a zero-betatron-amplitude particle are $v_x = 1.82$ and $v_z = 1.85$. Although the vacuum chamber is elliptically shaped, we calculate the frequency map for the rectangular area $x \in (-50\text{ mm}, 50\text{ mm})$ and $y \in (0, 25\text{ mm})$. We use 15,000 particles uniformly distributed in the area. Systematic dipole errors with $K_1 = -0.003037\text{m}^{-2}$, $K_2 = 0.0575958\text{m}^{-3}$ and $K_3 = 20\text{m}^{-4}$ are used in the simulation. Because the quadrupole and sextupole errors do not produce systematic resonances, their effects are not important. Only the systematic octupole field is important to the dynamics. There is no particle loss in this simulation. Here, we note that the betatron tunes are trapped on the resonance line with a substantial decrease in the diffusion index. The decrease of diffusion index is not a surprise owing to the trapping of these particles on the resonance line. A supplementary .gif file shows the evolution of the frequency map and diffusion index for every 100 revolutions. It shows the converging of the betatron tune toward the coupling line owing to the resonance and the decrease in diffusion index in the aperture. It would be interesting to know what happens to those particles trapped in the coupling resonance.

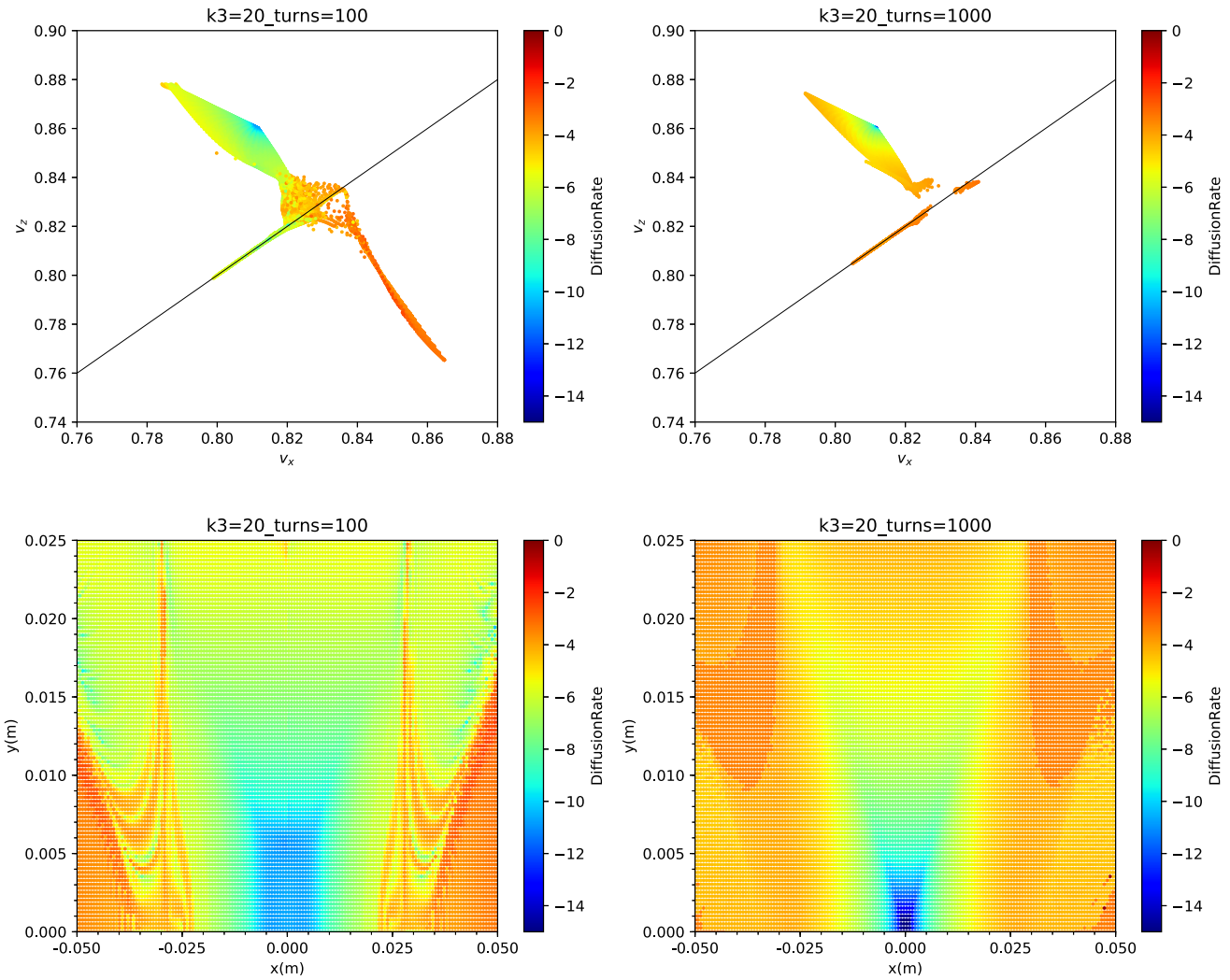

Fig. 2 (Color figure online) Top plots: Diffusion index versus the particle tunes at turn number 100 (left) and 1000 (right). Note that the tunes of the particles are trapped on the $2\nu_x - 2\nu_z = 0$ resonance. The betatron tunes of the zero-amplitude particles are $\nu_x = 1.82$ and $\nu_z = 1.85$. Bottom plots: the corresponding diffusion index versus the horizontal aperture ± 50 mm and vertical aperture 0–25 mm

3 Effects of the octupole coupling resonance on beam dynamics

To understand the effect of the octupole resonances, we perform a Floquet transform on the Hamiltonian in Eq. (1) [22]:

$$x = \sqrt{2\beta_x J_x}\cos(\psi_x + \chi_x(s) - \nu_x\theta),$$
$$z = \sqrt{2\beta_z J_z}\cos(\psi_z + \chi_z(s) - \nu_z\theta),$$

where (J_x, ψ_x) and (J_z, ψ_z) are conjugate action-angle coordinates, ν_x and ν_z are betatron tunes and $\chi_{x,z} = \int_0^s \frac{1}{\beta_{x,z}(s)}\mathrm{d}s$ are betatron phase advances. The resulting Hamiltonian is

$$H = \nu_x J_x + \nu_z J_z + \frac{1}{2}\alpha_{xx}J_x^2 + \alpha_{xz}J_xJ_z + \frac{1}{2}\alpha_{zz}J_z^2 + G_{2,-2,\ell}J_xJ_z\cos(2\phi_x - 2\phi_z - \ell\theta + \xi_{2,-2,\ell}) + \cdots, \quad (2)$$

where the orbiting angle, $\theta = s/R$, serves as the "time coordinate," R is the mean radius, ℓ is an integer, α_{xx}, α_{xz} and α_{zz} are nonlinear detuning parameters and $G_{2,-2,\ell}$ and $\xi_{2,-2,\ell}$ are the resonance strength and its phase, given by

$$\alpha_{xx} = \frac{1}{16\pi}\oint \beta_x^2 K_3 \mathrm{d}s, \quad \alpha_{xz} = \frac{-1}{8\pi}\oint \beta_x\beta_z K_3 \mathrm{d}s,$$
$$\alpha_{zz} = \frac{1}{16\pi}\oint \beta_z^2 K_3 \mathrm{d}s, \quad G_{2,-2,\ell}e^{j\xi_{2,-2,\ell}}$$
$$= \frac{1}{16\pi}\oint \beta_x\beta_z K_3(s)\times e^{j[2\chi_x(s)-2\chi_z(s)-(2\nu_x-2\nu_z-\ell)\theta]}\mathrm{d}s,$$

where β_x and χ_x are the horizontal betatron function and betatron phase and $\beta_z(s)$ and $\chi_z(s)$ are those of the vertical betatron motion. Figure 3 shows the detuning parameters and the octupole coupling resonance versus the integrated octupole field in a dipole of the XiPAF, and the resonance phase is $\xi_{2,-2,0} = 60°$. To understand the effect of the coupling resonance on beam dynamics, we perform a canonical transformation to this coupling Hamiltonian using the generating function:

$$F_2(\phi_x,\phi_z,J_1,J_2) = \left(\phi_x - \phi_z - \frac{1}{2}\ell\theta + \frac{1}{2}\xi_{2,-2,\ell}\right)J_1 + \phi_z J_2.$$

The coordinate transformation from the old phase-space coordinates to the new phase-space coordinates is

$$\phi_1 = \phi_x - \phi_z - \frac{1}{2}\ell\theta + \frac{1}{2}\xi_{1,-2,\ell}, \quad J_x = J_1,$$
$$\phi_2 = \phi_z, \quad J_z = -J_1 + J_2,$$

and the new Hamiltonian becomes $\tilde{H} = H_1(J_1,\phi_1,J_2) + H_2(J_2)$, where $H_2(J_2) = \nu_z J_2 + \frac{1}{2}\alpha_{22}J_2^2$ and

$$H_1(J_1,\phi_1,J_2) = \delta J_1 + \frac{1}{2}\alpha_{11}J_1^2 + \alpha_{12}J_1J_2 + G_{2,-2,\ell}J_1(J_2-J_1)\cos(2\phi_1). \tag{3}$$

Here, $\delta = \nu_x - \nu_z - \frac{1}{2}\ell$ is the resonance proximity parameter, and the detuning parameters are $\alpha_{11} = \alpha_{xx} - 2\alpha_{xz} + \alpha_{zz}$, $\alpha_{12} = \alpha_{xz} - \alpha_{zz}$, and $\alpha_{22} = \alpha_{zz}$. Hamilton's equations of motion are $\frac{\mathrm{d}J_2}{\mathrm{d}\theta} = -\frac{\partial\tilde{H}}{\partial\phi_2} = 0$, $\frac{\mathrm{d}\phi_2}{\mathrm{d}\theta} = \frac{\partial\tilde{H}}{\partial J_2}$, and

$$\frac{\mathrm{d}J_1}{\mathrm{d}\theta} = -\frac{\partial\tilde{H}}{\partial\phi_1} = +2G_{2,-2,\ell}J_1(J_2-J_1)\sin(2\phi_1), \tag{4}$$

$$\frac{\mathrm{d}\phi_1}{\mathrm{d}\theta} = \frac{\partial\tilde{H}}{\partial J_1} = \{\delta + \alpha_{12}J_2\} + \alpha_{11}J_1 + G_{2,-2,\ell}(J_2-2J_1)\cos(2\phi_1). \tag{5}$$

Particle dynamics obey Eqs. (4) and (5) at constant J_2 and H_1, which are invariant if the bare betatron tunes ν_x and ν_z do not vary with time. Particle motion in the horizontal and the vertical planes is coupled as shown in the dynamic-aperture study in Sect. 2, where particle tunes are shown to "damp" to the resonance line.

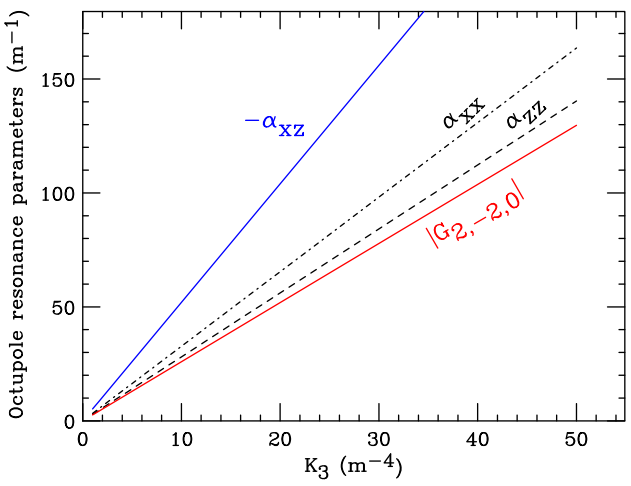

Fig. 3 The detuning parameters and the strength of the octupole coupling resonance for the XiPAF is drawn as a function of the octupole integrated field in the dipole

3.1 Fixed points and separatrices

Because the Hamiltonian H_1 is also invariant, each invariant torus in the phase-space coordinates,

$$X_1 = \sqrt{2\beta_x J_1}\cos\phi_1, \quad P_1 = -\sqrt{2\beta_x J_1}\sin\phi_1, \tag{6}$$

of the resonance rotating frame will have constant H_1 and J_2 values. The tori can be analyzed by the fixed points and separatrix of the Hamiltonian.

The fixed points are determined by solving $\mathrm{d}J_1/\mathrm{d}\theta = 0$ and $\mathrm{d}\phi_1/\mathrm{d}\theta = 0$:

$$2G_{2,-2,\ell}J_1(J_2-J_1)\sin(2\phi_1) = 0, \tag{7}$$

$$\{\delta + \alpha_{12}J_2\} + \alpha_{11}J_1 + G_{2,-2,\ell}(J_2-2J_1)\cos(2\phi_1) = 0. \tag{8}$$

The unstable fixed points (UFP) are located at

$$J_{1,\mathrm{UFP}} = J_2; \quad \cos(2\phi_{1,\mathrm{UFP}}) = \frac{\delta + (\alpha_{12}+\alpha_{11})J_2}{G_{2,-2,\ell}J_2}, \tag{9}$$

provided that $|\delta + (\alpha_{12}+\alpha_{11})J_2| \le |G_{2,-2,\ell}J_2|$. The separatrix is the Hamiltonian torus that passes through the UFP, i.e., $J_1 = J_2$ and

$$\delta + \frac{1}{2}\alpha_{11}(J_1+J_2) + \alpha_{12}J_2 - G_{2,-2,\ell}J_1\cos(2\phi_1) = 0. \tag{10}$$

This is an ellipse in the normalized phase-space coordinates (X_1, P_1). The UFP of Eq. (9) is the intersection of the separatrix of Eq. (10) and the Courant–Snyder circle $J_1 = J_2$.

The stable fixed points (SFP) are located at

$$\delta + \alpha_{12}J_2 + \alpha_{11}J_{1,\mathrm{SFP}} \pm G_{2,-2,\ell}(J_2 - 2J_{1,\mathrm{SFP}}) = 0, \tag{11}$$

where the $\pm$ corresponds to $\phi_{1,\mathrm{SFP}} = 0$ or π, and $\pi/2$ or $3\pi/4$, respectively. Depending on the value of J_1 and J_2 of the beam particles, particles locked onto the resonance will have their own separatrices.

For particles not trapped on the resonance, their ellipses are simply regular Courant–Snyder invariants. Alternatively, for particles trapped on the resonance line, their ellipses are divided into two halves by a coupling ellipse of Eq. (10), where the curvature is determined by α_{11} and $G_{2,-2,\ell}$. Because particle actions J_x and J_z are coupled, the horizontal and vertical beam emittances can exchange unless the initial emittances are equal: $\epsilon_{xi} = \epsilon_{zi}$ [23].

3.2 Numerical simulations

To demonstrate the effect of the coupling resonance on beam particles, we track a beam with 50 particles at an accelerator with parameters $\alpha_{xx} = 727.24\mathrm{m}^{-1}$, $\alpha_{xz} = -1256.78\mathrm{m}^{-1}$, $\alpha_{zz} = 727.24\mathrm{m}^{-1}$ and $|G_{2,-2,0}| = 628.39\mathrm{m}^{-1}$. The bare betatron tunes are $\delta = \nu_x - \nu_z = -0.02$.

Figure 4 shows the "instantaneous tunes" and the normalized phase-space Poincaré maps in the resonance rotating frame of 50 particles every 100 turns. Here, the instantaneous fractional tune is defined as

$$q_x(n) = \frac{\psi_x(n) - \psi_x(n-1)}{2\pi}, \tag{12}$$

$$q_z(n) = \frac{\psi_z(n) - \psi_z(n-1)}{2\pi}. \tag{13}$$

Note that there are ten particles locked onto the coupling resonance and their Poincaré maps have a characteristic resonance structure. Their instantaneous betatron tunes have the specific feature of locking onto the resonance line with tune modulation depending on their amplitude. Although the frequency-map analysis [10–12] put the tunes of these particles on the coupling line, as shown in the top plots of Fig. 2, the instantaneous betatron tunes oscillate around the resonance line, but not on the resonance line.

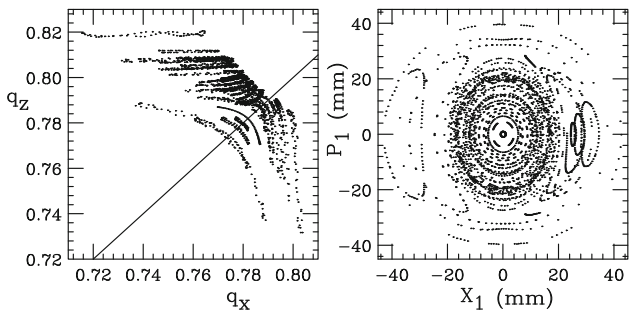

Fig. 4 Left: The vertical tune versus the horizontal tune of 50 particles is plotted for every 100 revolutions for 6100 revolutions. Right: The evolution of the phase-space Poincaré map (X_1, P_1) of these 50 particles

The right plot of Fig. 4 shows the normalized Poincaré map of these 50 particles at every 100 revolutions for 6100 revolutions. It is clear that particles locked onto resonances having invariant tori separated by their separatrices, as shown in Eq. (10).

4 Conclusion

We performed a dynamic-aperture analysis of the XiPAF in the presence of systematic octupoles in dipole magnets. Although the fourth-order coupling resonance is relatively strong, the coupling resonance will not affect the DA of this compact accelerator. Using the frequency-map analysis, we showed that the tune "damping" to the resonance line is associated with the principle frequency analysis of the software. The betatron tunes of these trapped particles are actually still varying largely turn-by-turn. The apparent tune "damping" is essentially the artifact of tune computation (see Fig. 2).

References

1. S.X. Zheng, Q.Z. Xing, X.L. Guan et al., Overall design and progress of XiPAF project, in *Proceedings of SAP2017* (WECH2, Jishou, 2017). https://doi.org/10.18429/JACoW-SAP2017-WECH2
2. G.R. Li, S.X. Zheng, H.J. Yao et al., Design of a compact ring for proton radiation applications. Chin. Phys. C **41**(1), 017001 (2017). https://doi.org/10.1088/1674-1137/41/1/017001
3. S.X. Zheng, Q.Z. Xing, X.L. Guan et al., Design of the 230 MeV proton accelerator for Xi'an proton application facility, in *Proceedings of HB2016* (MOPR006, Malmo, 2016). https://doi.org/10.18429/JACoW-HB2016-MOPR006
4. H.J. Yao, S.X. Zheng, G.R. Li et al., H-charge exchange injection for XiPAF synchrotron, in *Proceedings of HB2016* (MOPR004, Malmo, 2016). https://doi.org/10.18429/JACoW-HB2016-MOPR004
5. H.J. Yao, G.R. Li, Q. Zhang et al., RF-Knockout slow extraction design for XiPAF synchrotron, in *Proceedings of HB2016* (MOPR005, Malmo, 2016). https://doi.org/10.18429/JACoW-HB2016-MOPR005
6. B.W. Montague, Fourth-order coupling resonance excited by space-charge forces in a synchrotron. in *CERN-Report No. 68-38, CERN* (1968)
7. I. Hofmann, G. Franchetti, J. Qiang et al., Dynamical effects in crossing of the montague resonance, in *Proceedings of EPAC04* (WEPLT053, Lucerne, 2004)
8. S. Ohnuma, R.L. Gluckstern, Width of nonlinear difference resonances. IEEE Trans. Nucl. Sci. **32**(5), 2261 (1985). https://doi.org/10.1109/TNS.1985.4333879
9. G.R. Li, *Study of the Key Physics and Technology Problems of a Compact Proton Synchrotron for Radiation Applications*. Ph.D. Thesis, Tsinghua University (2017)
10. J. Laskar, Frequency analysis for multidimensional systems-global dynamics and diffusion. Physica D **67**, 257 (1993). https://doi.org/10.1016/0167-2789(93)90210-R

11. J. Laskar, D. Robin, Application of frequency map analysis to the ALS. Part. Accel. **54**, 183 (1996)
12. L. Nadolski, J. Laskar, Review of single particle dynamics for third generation light sources through frequency map analysis. Phys. Rev. Accel. Beams **6**, 114801 (2003). https://doi.org/10.1103/PhysRevSTAB.6.114801
13. J. Laskar, Frequency map analysis and particle accelerators, in *Proceedings of PAC03*, vol. 378 (Portland, 2003). https://doi.org/10.1109/PAC.2003.1288929
14. S.A. Antipova, S. Nagaitsevb, A. Valishevb, Single-particle dynamics in a nonlinear accelerator lattice: attaining a large tune spread with octupoles in IOTA. J. Instrum. **12**, P04008 (2017). https://doi.org/10.1088/1748-0221/12/04/P04008
15. Y. Wang, M. Ball, B. Brabson et al., Effects of tune modulation on particles trapped in one-dimensional resonance islands. Phys. Rev. E **49**, 5697 (1994). https://doi.org/10.1103/PhysRevE.49.5697
16. M. Ball, B. Brabson, J. Budnick et al., Beam motions near separatrix, in *Proceedings of PAC1999*, vol. 1548 (New York, 1999). https://doi.org/10.1109/PAC.1999.794169
17. M. Borland, Elegant: a flexible SDDS-compliant code for accelerator simulation, in *Proceedings of ICAP2000* (LS-287, Darmstadt, 2000)
18. M. Borland, Features and applications of the program ELEGANT, in *Proceedings of IPAC2013* (THPPA02, Shanghai, 2013)
19. M. Borland, ElegantRingAnalysis: an interface for high-throughput analysis of storage ring lattices using elegant, in *Proceedings of PAC2005* (Knoxville, Tennessee, 2005), p. 4200. https://doi.org/10.1109/PAC.2005.1591764
20. Y.-R.E. Tan, M.J. Boland, G. LeBlanc, Applying frequency map analysis to the Australian synchrotron storage ring, in *Proceedings of PAC2005* (Knoxville, Tennessee, 2005), p. 407. https://doi.org/10.1109/PAC.2005.1590448
21. Z. Nergiz, A. Aksoy, Low emittance lattice for the storage ring of the Turkish Light Source Facility TURKAY. Chin. Phys. C **39**(6), 067002 (2015). https://doi.org/10.1088/1674-1137/39/6/067002
22. S.Y. Lee, *Accelerator Physics*, 3rd edn. (World Scientific, Singapore, 2011)
23. S.Y. Lee, K.Y. Ng, H. Liu et al., Evolution of beam distribution in crossing a walkinshaw resonance. Phys. Rev. Lett. **110**, 094801 (2013). https://doi.org/10.1103/PhysRevLett.110.094801